HHS Public Access

Author manuscript

Leukemia. Author manuscript; available in PMC 2016 May 18.

Published in final edited form as:

Leukemia. 2016 February ; 30(2): 390–398. doi:10.1038/leu.2015.229.

Blocking the ZZ Domain of Sequestosome1/p62 Suppresses Myeloma Growth and Osteoclast Formation In Vitro and Induces Dramatic Bone Formation in Myeloma-Bearing Bones In Vivo

Jumpei Teramachi[1,‡], **Rebecca Silbermann**[1,‡,*], **Peng Yang**[2,3,‡], **Wei Zhao**[1], **Khalid S. Mohammad**[4], **Jianxia Guo**[5], **Judith L. Anderson**[1], **Dan Zhou**[1], **Rentian Feng**[2], **Kyaw-Zeyar Myint**[2], **Nathan Maertz**[6], **Jan H. Beumer**[2,7], **Julie L. Eiseman**[5,7], **Jolene J. Windle**[8], **Xiang-Qun Xie**[2,‡‡], **G. David Roodman**[1,9,‡‡], and **Noriyoshi Kurihara**[1,‡‡]

[1]Department of Medicine, Hematology Oncology, Indiana University, Indianapolis, IN

[2]Department of Pharmaceutical Sciences, University of Pittsburgh, Pittsburgh, PA

[3]Computational Chemical Genomics Screening Center, University of Pittsburgh, Pittsburgh, PA

[4]Department of Medicine, Division of Endocrinology, Indiana University, Indianapolis, IN

[5]Department of Pharmacology Chemical Biology, University of Pittsburgh, Pittsburgh, PA

[6]Department of Radiology, Indiana University, Indianapolis, IN

[7]Molecular Therapeutics/Drug Discovery Program, University of Pittsburgh, Pittsburgh, PA

[8]Department of Human and Molecular Genetics, Virginia Commonwealth University, Richmond, VA

[9]Richard L. Roudebush VA Medical Center, Indianapolis, IN

Abstract

We reported that p62 (sequestosome 1) serves as a signaling hub in bone marrow stromal cells (BMSC) for the formation of signaling complexes, including NFκB, p38MAPK, and JNK, that are involved in the increased osteoclastogenesis and multiple myeloma (MM) cell growth induced by BMSC that are key contributors to myeloma bone disease (MMBD), and demonstrated that the

*Contact Author: Rebecca Silbermann MD, Hematology Oncology, Department of Medicine, Indiana University, 980 W Walnut Street, C310, Indianapolis, Indiana 46202.

‡Equal contributions as 1st author

‡‡Co-corresponding authors

Conflicts of Interest

G.D.R. is a consultant for Amgen. X.Q.X. is a consultant for Oxis Biotech. The remaining authors declare no competing financial interests.

Authorship Contributions

J.T. and N.K. designed and performed in vitro research and analyzed and interpreted data; P.Y., R.F., K.M., and X.X. designed, synthesized, and characterized XRK3F2; R.S. and W.Z. performed μCT analysis to characterize new bone formation; K.S.M. performed histology and immunohistochemistry; N.M. interpreted radiographs; J.G., J.H.B., and J.L.E. designed, performed and analyzed in vivo pharmacokinetic and pharmacodynamic experiments; J.J.W. provided C57BL/KaLwRij mice; and R.S. and G.D.R. designed the research, analyzed and interpreted data, and wrote the manuscript.

Supplementary information is available at Leukemia's website.

ZZ-domain of p62 (p62-ZZ) is required for BMSC enhancement of MMBD. We recently identified a novel p62-ZZ inhibitor, XRK3F2, that inhibits MM cell growth and BMSC growth enhancement of human MM cells. In the current study we evaluate the relative specificity of XRK3F2 for p62-ZZ, characterize XRK3F2's capacity to inhibit growth of primary MM cells and human MM cell lines, and test the in vivo effects of XRK3F2 in the immunocompetent 5TGM1 MM model. We found that XRK3F2 induces dramatic cortical bone formation that is restricted to MM containing bones and blocked the effects and upregulation of TNFα, an OBL differentiation inhibitor that is increased in the MM bone marrow microenvironment and utilizes signaling complexes formed on p62-ZZ, in BMSC. Interestingly, XRK3F2 had no effect on non-MM bearing bone. These results demonstrate that targeting p62 in MM models has profound effects on MMBD.

Keywords

Myeloma; Bone; Osteoblast; Osteoclast; Sequestosome 1; p62

Introduction

Multiple myeloma (MM) is a plasma cell malignancy marked by monoclonal protein production and lytic bone disease that is a major cause of patient morbidity. MM bone disease (MMBD) is marked by increased osteoclast (OCL) activity and highly suppressed or absent osteoblast (OB) activity. Adhesive interactions between MM cells and bone marrow stromal cells (BMSC) activate multiple signaling pathways in BMSC that enhance tumor growth and bone destruction while suppressing new bone formation and contributing to chemoresistance ([1–5]).

We reported that p62 (sequestosome 1) serves as a signaling hub in BMSC for the formation of signaling complexes involved in the BMSC-induced increase in osteoclastogenesis and MM cell growth characteristic of MMBD ([6]), including NFκB, p38MAPK, and JNK (Figure 1A), and recently demonstrated that the ZZ-domain of p62 (p62-ZZ) is required for BMSC enhancement of MMBD ([7]). We recently identified a novel p62-ZZ inhibitor, XRK3F2 (Figure 1B), using 3D homology modeling to predict the structure of the p62 protein and virtual screening molecular docking studies ([8]), and tested XRK3F2's potential to inhibit MM cell growth and modulate the MM bone marrow microenvironment. We found that XRK3F2 inhibited murine MM cell growth, BMSC-enhancement of human MM cell growth, and TNFα-induced OCL formation by WT but not $p62^{-/-}$ OCL precursors, and that it's effects were specific to p62 ([9]).

The current study evaluates the relative specificity of XRK3F2 for p62-ZZ, XRK3F2's growth inhibition of human MM cell lines and primary human MM cells, and characterizes the in vivo efficacy of XRK3F2 in the immunocompetent 5TGM1 MM model. We report that XRK3F2 induces new bone formation in areas of high MM burden without altering non-tumor bearing bone. To evaluate potential mechanisms by which XRK3F2 induces bone formation, we tested the effects of XRK3F2 on osteoblast (OB) differentiation and MM cell – stromal cell (pre-OB) interactions.

Materials and Methods

Isolation of human bone marrow cells and BMSC

After obtaining informed consent, marrow aspirates were obtained from MM patients and healthy subjects. These studies were approved by the University of Pittsburgh and Indiana University IRBs. Marrow mononuclear cells were isolated and depleted of non-adherent cells as previously described ([10], [11]) and enriched for OCL precursors by CD11b MicroBead® selection (Miltenyi Biotec Inc., Auburn, CA). Adherent cells were processed as described ([12]) and used at passages 2 to 3. Human MM cells (>90% purity) were isolated by magnetic cell fractionation using anti-CD138 MicroBeads® (Miltenyi Biotec Inc.) and used for experiments described below. ([13]).

Osteoclast formation assays

$CD11b^+$ cells were cultured with 10 ng/ml TNFα or 50 ng/ml RANKL for 48h for Western analyses, or for 21d for osteoclastogenesis assays, as described ([10]). 23C6 positive multinuclear cells (containing at least 3 nuclei) were scored as OCL ([14]).

Myeloma cell lines

MM cell lines was generously provided by Drs. Steven Rosen (MM1.S), Babatunde O. Oyajobi (5TGM1), Diane Jelinek (ANBL-6) Nicola Giuliani (JJN3), Suzanne Lentzsch (RPMI8226), and Louis Stancato (U266, H929). 5TGM1 cells were stably transfected with a lentiviral construct containing GFP (5TGM1-gfp) and maintained as previously described ([12]).

OB differentiation assays

Primary BMSC or MC4 cells were cultured under osteogenic conditions in the presence or absence of 5TGM1 cells as described ([12]). Relative expression of key OB differentiation genes was quantified using real-time PCR, as described ([12]). GAPDH and 18S were used as internal controls.

Cell proliferation assays

Primary MM cells, human MM cell lines, or murine 5TGM1-gfp cells were incubated in 96-well plates in RPMI-1640 media with 10% FCS and varying concentrations of XRK3F2 for 48h (human MM cell lines and primary MM cells) or 72h (murine MM cells). Viable cells were quantified by MTT assay (Sigma-Aldrich, St. Louis, MO), per the manufacturer. The IC_{50} was calculated from triplicate independent experiments using the Hill equation and the ADAPT 5 program ([15]).

Western blot analyses

BMSC or OCL precursor cell lysates were loaded onto 7.5% sodium dodecyl sulfate polyacrylamide gels (SDS-PAGE) (for V-CAM1 expression) or 10% SDS-PAGE (for cell signaling analyses) and electrophoresed under reducing conditions using precast gels (Bio-Rad Laboratories, Hercules, CA), as described ([16]). Antibodies used for immunoblotting included: anti-phospho PKCζ (Thr410/403), anti-phospho IκBα (Ser32), anti-phospho p38

MAPK (Thr180/Tyr182) and anti-p38 MAPK, anti-PKCξ, anti-IκBα, cleaved and uncleaved caspases 3, 7, and 9 (all from Cell Signaling, Boston, MA, catalog numbers 9378, 2859, 9211, 9212, 9368, 9242, respectively), anti-c-Fos, anti-NFATc1 and anti-V-CAM1 (Santa Cruz Biotechnology, Dallas, TX, catalog numbers sc-52, sc-7294, sc-1504, respectively), and anti-TNF-α (R&D Systems, Minneapolis, MN, catalog number AF-410-NA). β-actin was used for a control (Abcam, Cambridge, MA, catalog ab49900).

Human IL-6 and RANKL production

BMSC (2×10^5) were cultured in α-MEM-10% FCS for 48h and IL-6 and RANKL production in conditioned media (CM) was quantified using commercially available ELISA kits (IL-6, R&D Systems, and RANKL, ALPCO Immunoassays, Salem, NH), per the manufacturers' instructions.

Mice

Specific-pathogen-free, male C57BL/KaLwRij mice (6–12 weeks of age) were obtained from Dr. Jolene Windle at Virginia Commonwealth University. Mice were maintained and handled in accordance with the Guide for the Care and Use of Laboratory Animals ([17]) on a protocol approved by the University of Pittsburgh IACUC. For selected experiments, primary murine BMSCs were isolated from these mice and cocultured with MM cell lines, as described ([12]). BMSC from p62KO$^{-/-}$ mice and p62$^{+/-}$ littermates were isolated and maintained as previously described ([6]).

In vivo efficacy of XRK3F2

1×10^5 5TGM1-gfp cells in logarithmic phase growth were inoculated into one tibia (IT) of C57BL/KaLwRij mice under Nembutal anesthesia. Buprenorphine was administered as an analgesic 2h before and for 48h after tumor cell implantation. Supplemental Figure 1 provides a detailed schema for the in vivo studies. Briefly, animals were stratified by IgG_{2b} levels two weeks after tumor implantation and treated with either XRK3F2 (27 mg/kg/day or 40 mg/kg/day) or vehicle (0.01ml/g in 15% hydroxyl propyl β cyclodextrin in saline/day) intraperitoneally (IP) for 5 consecutive days/ week for 2 weeks. Mice were then followed for delayed effects for up to 2 weeks following treatment, or until tumors reached 2g. 12 animals were treated per group, based on our prior experience with tumor take in this model ([12]). Doses and dosing schedules were chosen based on preliminary multidose pharmacokinetic studies (data not shown).. Following euthanasia, blood was collected by cardiac puncture, bilateral tibias and femurs removed and fixed in 10% phosphate buffered formalin for 48 hours and then transferred to 70% ethanol.

IgG_{2b} concentrations

Plasma IgG_{2b} concentrations were determined using commercially available ELISA kits, according to manufacturer instructions (Bethyl Laboratories, Inc., Montgomery, TX).

Radiography and micro-computed tomography (μCT)

Radiographs of formalin fixed tibiae were obtained using an XPERT 80 Digital Cabinet X-ray System with energy range: 10-90 kV and tube current up to 1.0 mA (Kubtec Digital X-

ray, Milford, CT, USA), and analyzed by a blinded observer. New woven bone formation was quantified using a microCT system (viva CT 40, Scanco Medical, Brüttisellen, Switzerland). Details of μCT analysis are in the supplementary methods.

Histology and histomorphometry

Hind limbs were fixed as described above and decalcified in 10% EDTA for two weeks. Tissues were processed as previously described ([18]) and sections were stained with hematoxylin and eosin, and tartrate resistant alkaline phosphatase (TRAP). Tumor localization was confirmed with anti-GFP staining (Abcam). Sections were viewed on a Leica DM LB compound microscope outfitted with a Q-Imaging Micropublisher Cooled CCD color digital camera (W. Nuhsbaum Inc, McHenry, IL).

Statistical analyses

For cell culture and μCT studies results are expressed as mean ± standard deviation. Significance was evaluated using a two-tailed, unpaired Student's *t*-test. Representative data for experiments repeated a minimum of 3 times is shown. For in vivo studies, animal IgG2b concentrations and body weights were evaluated by ANOVA with pairwise comparisons using Dunnett's T-test, Tukey's and Fisher's exact test. Nonparametric analyses of median data were performed using Kruskall-Wallis, and pair-wise comparisons were conducted using the Mann-Whitney test. Significance was set at $p \leq 0.05$. Statistics were performed using Minitab statistical software (Minitab, State College, PA).

Results

Specificity of XRK3F2 for the ZZ domain of p62

p62 is composed of five domains that are critical for protein-protein interactions required for the formation of signaling complexes that play important roles in BMSC-support of MM cell growth and OCL formation (Figure 1A). We recently demonstrated that p62-ZZ is required for BMSC-enhancement of MMBD ([9]). Because BMSC-MM interactions increase TNFα in the MM microenvironment, and NFκB signaling is activated in BMSC as a result of MM cell – BMSC binding ([19]), we assessed the relative specificity of XRK3F2 for p62-ZZ domain of p62 by testing if XRK3F2 preferentially blocked TNFα rather than IL-1β-induced NFκB signaling, because TNFα utilizes the ZZ domain while IL-1β utilizes the TRAF6 domain of p62 to facilitate NFκB signaling. XRK3F2 blocked TNFα but not IL-1β stimulated NFκB phosphorylation in MM patient BMSC (Figure 2A) and inhibited IκBα degradation by interfering with p-IκBα activation in MM cells treated with TNFα (Figure 2B). XRK3F2 also significantly inhibited TNFα-enhanced VCAM-1, IL-6, and RANKL expression by BMSCs from MM patients compared to vehicle (Figures 2C–E).

XRK3F2 inhibits TNFα-induced osteoclast formation

To further assess the relative specificity of XRK3F2 for the ZZ domain, we next tested the effects of XRK3F2 on TNFα and RANKL-induced human OCL formation. We previously found that XRK3F2 inhibited TNFα-induced murine OCL formation by $p62^{+/-}$ but not $p62^{-/-}$ OCL precursors ([8]). XRK3F2 dose-dependently inhibited OCL formation by CFU-GM derived from $CD11b^{+}$ cells treated with TNFα at very low concentrations of XRK3F2

(0.1 μM) (Figure 3A). OCL formation induced by RANKL was only partially inhibited and required higher concentrations of XRK3F2 (1.0 to 10 μM). This was expected as RANKL signaling utilizes the TRAF6, p38MAPK, and ZZ domains of p62 to induce OCL formation ([6], [20]). Further, although high dose XRK3F2 (10μM) blocked OCL formation, it did not trigger caspase activation or other apoptosis-inducing factors in OCL precursors (data not shown). These results suggest that XRK3F2 predominantly inhibits OCL precursor differentiation.

We next assessed the effect of XRK3F2 on TNFα and RANKL-induced expression of OCL differentiation and activation factors in OCL precursors. Consistent with our data in BMSC and primary MM cells, XRK3F2 strongly inhibited TNFα, but only modestly blocked RANKL-induced c-Fos and NFATc1 expression (Figure 3B). To determine the mechanisms responsible for XRK3F2's inhibition of TNFα-induced OCL formation, we then examined the effects of XRK3F2 on downstream signaling pathways induced by TNFα in OCL precursors. XRK3F2 inhibited PKCζ and IκBα but not p38 MAPK activation in OCL precursors (Figure 3C), which utilizes the p38 domain of p62.

XRK3F2 directly inhibits the growth of MM cell lines and primary multiple myeloma cells but does not affect BMSC viability

As we previously reported that XRK3F2 inhibits growth of MM1.S human MM cells ([8]), we next evaluated the effects of XRK3F2 on 5TGM1 murine MM cell growth, the MM cell line used in our in vivo model of MMBD ([12]), 6 human MM cell lines, and primary MM cells. XRK3F2 significantly inhibited the growth of all 6 human MM cell lines, and primary human MM cells (Figure 4A, B). (Patient characteristics are summarized in the Table). The IC_{50} of XRK3F2 for 5TGM1 cells was 4.35μM (Figure 4C), and 4.6 μM for the human MM1.S cell line. In addition, 5TGM1 cells accumulated XRK3F2, with peak concentrations in the cell pellet of 370 μM after 30 min. Cell concentrations remained above 300 μM for 24 hours (Supplemental Figure 2).

We previously demonstrated that XRK3F2 inhibits murine MM cell growth and human BMSC-support of human MM cell growth ([7]). Therefore, we evaluated if XRK3F2 altered the viability and/or function of primary BMSCs from MM patients and healthy donors and the mechanism of it's effects on MM cells. XRK3F2 did not alter BMSC viability (data not shown). XRK3F2 induced apoptosis in MM cells, as demonstrated by cleavage of caspases 9, 7 and 3 after 16 hours (Figure 4D).

XRK3F2 induces new cortical bone formation in MMBD in vivo

Based on these encouraging results we examined the effects of XRK3F2 in an immunocompetent model of myeloma, as described in the Methods section and Supplemental Figure 1.

The $t_{1/2}$ of XRK3F2 in these mice was 10.3 hours (data not shown). Consistent with prior studies, 77% of evaluable animals inoculated with 5TGM1 cells (27 of 35) had MM engraftment, as defined by end of study elevation of plasma IgG_{2b} levels ([12])., ([12])Body weights and hematocrits did not differ among the treatment and control groups, or in animals receiving high and low XRK3F2 doses (data not shown). Plasma IgG_{2b} concentrations at the

end of dosing were higher in all groups as compared to at stratification, indicating that MM burden increased regardless of if animals received XRK3F2 or vehicle.

μCT and x-ray were used to evaluate bone disease in all animals at the end of the study. Six of 17 XRK3F2-treated and 1 vehicle-treated animal demonstrated a marked periosteal reaction on x-ray, suggesting new bone formation along the tibia (Figure 5A). However, μCT analysis of all animals demonstrated increased cortical bone in all XRK3F2 treated animals, as determined by the ratio of new cortical bone volume to total bone volume (N-BV/T-BV), independent of XRK3F2 dose (Figure 5C). μCT findings were confirmed by histology (Figure 6). Trabecular bone volumes did not differ between vehicle and XRK3F2 treated animals. Interestingly, no new bone formation was detected in the non-MM-bearing leg of XRK3F2-treated animals, (Figure 5E), indicating a lack of effect on bone not involved by MM. XRK3F2 treated animals with tumor burdens at the end of study (based on IgG_{2b} levels) displayed greater cortical bone formation than XRK3F2 treated animals with low tumor burden (Figure 5D). Further analyses demonstrated no reduction in the volume of the marrow cavity in animals with new cortical bone formation, suggesting that increased endocortical bone formation did not occur within the marrow space (data not shown).

Histologic analysis of tibiae confirmed the presence of new, woven bone, (bone that was laid down rapidly, Figure 6F), in XRK3F2-treated animals but not in vehicle treated animals (Figure 6A). The majority of the periosteal surface of the tibiae of these samples had new bone formation that was localized to one side (Figure 6B). Anti-GFP immunohistochemistry confirmed that MM cells closely apposed areas of new bone formation (Figure 6C). TRAP staining demonstrated osteoclasts in the new bone, indicating that bone remodeling occurred in the new bone (Figure 6E). No new trabecular bone was noted within the marrow cavity. Finally, in a pilot study, XRK3F2 did not induce new bone formation in mice that had not been injected with MM cells (data not shown).

XRK3F2 alters MM cell – BMSC cell interactions by reducing MM cell-derived TNFα in the myeloma microenvironment

To examine the mechanism responsible for the new bone formation observed in vivo, we evaluated if XRK3F2 alters production of known MM cell derived OB inhibitors, directly induces OB differentiation, or alters MM cell-induced suppression of OB differentiation.

5TGM1 cells were analyzed for their expression of IL-7 and TNFα, known suppressors of OB differentiation that are upregulated in the presence of BMSC. (In 5TGM1 cells DKK1 expression is not upregulated by BMSC, as previously reported ([12])). XRK3F2 did not induce TNFα or IL-7 in 5TGM1 cells cultured with XRK3F2, or induce OB differentiation of primary murine BMSCs or MC4 cells, a mouse calvarial pre-OB cell line, in the absence of MM cells, as assessed by expression of OB differentiation markers Ocn, ALP, and Runx2 (data not shown). These results suggest that XRK3F2 affects MM cell-BMSC interactions, rather than either cell type individually.

MM cell-BMSC interactions activate BMSC signaling pathways that inhibit OB differentiation ([6]). Therefore, we evaluated if XRK3F2 alters MM cell-induced inhibition of OB differentiation. MC4 cells were cocultured with 5TGM1 cells under osteogenic

conditions with or without XRK3F2. Coculture of MC4 cells with 5TGM1 cells suppressed Runx2 mRNA expression in MC4 cells. However, Runx2 expression in MC4 cells cocultured with MM cells and XRK3F2 was significantly higher than Runx2 expression in MC4 cells cocultured with MM cells in the absence of XRK3F2 (Figure 7A), demonstrating that XRK3F2 blocked MM cell induced suppression of OB differentiation.

Because XRK3F2 blocks TNFα-mediated OCL formation, and TNFα is a major suppressor of OB differentiation that is upregulated in the marrow microenvironment by MM cell–stromal cell interactions, we hypothesized that XRK3F2 reduces OB suppression (allowing differentiation) in the MM bone marrow microenvironment by altering production of TNFα. 5TGM1 cells were cocultured with mBMSC in the presence or absence of XRK3F2. At the end of the culture period, TNFα expression in 5TGM1 cells and mBMSC was evaluated by qPCR. TNFα mRNA expression was significantly upregulated in both 5TGM1 cells and BMSCs following coculture. Interestingly, XRK3F2 prevented coculture-induced upregulation of TNFα mRNA in 5TGM1 cells (Figure 7B) and mBMSC. in BMSCs. To confirm these findings at the protein level, and to determine if this reduction in TNFα upregulation was mediated by inhibition of p62 signaling, we repeated the experiment using BMSC from p62KO ($p62^{-/-}$) and $p62^{+/-}$ mice. TNFα expression was upregulated in $p62^{+/-}$ BMSC cocultured with 5TGM1 cells, and XRK3F2 reduced this upregulation by 40% after 12 hours of treatment. The upregulation of TNFα observed following coculture of $p62^{-/-}$ BMSC and 5TGM1 was only modestly reduced (20%) by XRK3F2 (Figure 7C). These findings are consistent with our prior data that XRK3F2 targets p62, and suggest that XRK3F2's effect on stromal cell-induced TNFα upregulation in MM cells and BMSCs requires p62.

Discussion

MMBD is characterized by an uncoupling of bone remodeling and persistent OBL suppression ([5]) that results in pathologic fractures and severe bone pain. Current treatment strategies focus on OCL inhibition, and to date no bone anabolic agent in MM has been identified that results in significant new bone formation in MM lesions. We recently reported that p62 plays a critical role in BMSC support of MM cell growth and OCL formation ([9]) and identified the p62-ZZ domain, a RIP binding domain involved in atypical PKC and NFkB signaling induced by TNFα ([21]), as a potential therapeutic target for MM and MMBD.

In this study we demonstrate that XRK3F2, a novel small molecule antagonist of the p62-ZZ domain ([9]), inhibited the growth of primary $CD138^{+}$ MM cells and human MM cell lines by inducing apoptosis, did not inhibit BMSC growth or induce BMSC apoptosis in an immunocompetent model of MMBD. Importantly, XRK3F2 induced dramatic, local new bone formation in bones bearing MM in vivo but did not induce new bone formation in bones from the same animals that were not directly inoculated with MM cells. The results demonstrate that XRK3F2 alters the effect of MM on bone.

Possible mechanisms for the bone anabolic effects we observed include direct effects of XRK3F2 on OBL or decreased production of OBL inhibitory factors by MM cells. Direct

effects of XRK3F2 on OBL are unlikely, as preliminary studies of XRK3F2 on OBL precursors in the absence of MM cells did not change OBL differentiation (data not shown), and XRK3F2 did not have an anabolic effect on bones without tumor. XRK3F2 treatment of MM cells also did not alter production of MM cell-derived OBL inhibitory factors, including TNFα and IL-7. Interestingly however, coculture of 5TGM1 cells with MC4 cells under osteogenic conditions in the presence of low concentrations of XRK3F2 resulted in upregulation rather than suppression of stromal cell Runx2, a critical transcription factor required for OBL differentiation that is normally suppressed with MM cell coculture (Figure 7A) ([12], [22]).

These data suggest that XRK3F2 induces new bone formation by blocking the effects of MM cell-derived inhibitors of OBL differentiation in BMSC, such as TNFα, which use signaling complexes formed on the ZZ-domain of p62. In support of this hypothesis, we found that XRK3F2 decreased primary MM patient BMSC production of VCAM-1 (Figure 3A), which mediates adhesive interactions between BMSCs and $\alpha_4\beta_1$ integrin on MM cells ([23]) and plays an important role in BMSC support of tumor growth and MMBD ([1], [6], [24]–[26]), via it's effects on TNFα-induced RANKL, and IL-6 (Figures 2D, 2E). Our finding that XRK3F2 blocked TNFα induced PKCς and IκBα phosphorylation in BMSCs when the cells were pre-treated with XRK3F2 ([27]), but only partially blocked IL-6 and RANKL production, suggests that both NFκB and p38MAPK signaling regulate IL-6 and RANKL production by TNFα in BMSCs. Additionally, we previously reported that IL-6 and RANKL production are dependent on both p38MAPK and NFκB signaling in MM patient BMSCs ([6]). These results suggest that XRK3F2 may block the TNFα-induced suppression of OBL differentiation observed in MM cell–BMSC co-cultures ([28]), as XRK3F2 blocks TNFα mediated signaling in BMSC (Fig 3B), and upregulation of TNFα in both MM cells and BMSC when they are co-cultured (Figure 7B, C).

Importantly, OCL were present in the newly formed bone observed in our study. This demonstrates that the new bone had undergone active remodeling that could become normal lamellar bone over time, and that OCL activity in areas of new bone formation is not inhibited. It is likely that the OCL activity seen in the presence of XRK3F2 is induced by RANKL, as RANKL induction of OCL formation is dependent on both TRAF6 (TBS domain of p62) and p38MAPK (p38 domain of p62) signaling ([6], [20]). Consistent with this, XRK3F2 only modestly inhibited RANKL-induced OCL formation in vitro (Figure3A), though low concentrations of XRK3F2 inhibited TNFα – induced OCL formation. In addition, XRK3-F2 blocked OCL precursor differentiation to a lesser extent in the presence of RANKL (Figure 3C), but did not induce precursor apoptosis (XRK3F2 did not trigger caspase activation or induce apoptosis in OCL precursors, data not shown). This suggests that p62 is critical for normal human OCL precursor differentiation but not survival, and is supported by the finding that p62KO mice have normal basal OCL formation ([29]).

In our study, new woven bone formation occurred outside of the marrow space adjacent to tumor, and was seen only in bones that had been directly inoculated with MM cells. Since OBL suppression by MM is a local event, the proximity of new bone to tumor is consistent with the hypothesis that XRK3F2 alters MM suppression of OBL, suggesting that XRK3F2 allowed MM-exposed OBL to respond to anabolic stimuli released or expressed by OCL

during bone remodeling, and that OCL activity may be required for the anabolic effects of XRK3F2.

The results of XRK3F2 on MM cells in vitro also likely reflect a decrease in NFκB signaling. XRK3F2 directly activated caspases 3, 7, and 9 in MM cells (Figure 4D) and decreased NFκB signaling in MM results in the aggregation of caspase 8 and its downstream effector caspases ([30]). Thus, high concentrations of XRK3F2 induced apoptosis in MM cells. The immunocompetent MMBD model used to evaluate the efficacy of XRK3F2 in this study used animals with well-established disease (animals were implanted with MM cells 14 days prior to treatment initiation), and end of treatment serum IgG2b levels were significantly higher than levels at stratification, demonstrating continued tumor growth. This was expected, as plasma concentrations of XRK3F2 were not maintained above the IC_{50} for murine MM cells (4.35 μM) for more than 30 minutes following the 40mg/kg dose. The continued tumor growth resulted in extensive bone destruction and osteolysis throughout the marrow space in both vehicle treated and XRK3F2 treated animals.

To our knowledge, p62 has not been previously targeted in BMSCs or myeloma cells to prevent tumor progression and bone destruction. We suggest that targeting p62 in MM may be an attractive therapeutic strategy with little or no obvious nonspecific toxicity, as our preliminary data suggests that targeting p62 should not block normal hematopoiesis ([9]), and $p62^{-/-}$ mice have no phenotype aside from adult onset diabetes ([31]). We anticipate that XRK3F2 or its derivatives, in combination with more potent anti-myeloma agents such as bortezomib ([32], [33]), should have a profound therapeutic effect on MMBD.

Supplementary Material

Refer to Web version on PubMed Central for supplementary material.

Acknowledgments

The authors thank Drs. Rosen, Oyajobi, Giuliani, Stancato, and Jelinek for MM cell lines. This project used the University of Pittsburgh Cancer Institute (UPCI) Clinical Pharmacology Analytical Facility (CPAF) and UPCI Small Animal Facility, supported, in part, with funding from NIH-NCI Cancer Center Support Grant P30 CA047904. Services and products in support of the research project were also generated by the VCU Massey Cancer Center Transgenic/Knock-out Mouse Facility, supported, in part, with funding from NIH-NCI Cancer Center Support Grant P30 CA016059. Funding was also received from the Multiple Myeloma Research Foundation (N.K. and G.D.R.), the NIH R21CA141426, 5R01AR059679-05, 5R21CA179017-02 (G.D.R.) and R01DA025612, R21HL109654 (X.X.), and VA Merit Review Grant 5101CX000623-04 (G.D.R.).

References

1. Michigami T, Shimizu N, Williams PJ, Niewolna M, Dallas SL, Mundy GR, et al. Cell-cell contact between marrow stromal cells and myeloma cells via VCAM-1 and alpha(4)beta(1)-integrin enhances production of osteoclast-stimulating activity. Blood. 2000; 96(5):1953–1960. [PubMed: 10961900]
2. Sanz-Rodriguez F, Teixido J. VLA-4-dependent myeloma cell adhesion. Leukemia & lymphoma. 2001; 41(3–4):239–245. [PubMed: 11378537]
3. Okada T, Hawley RG, Kodaka M, Okuno H. Significance of VLA-4-VCAM-1 interaction and CD44 for transendothelial invasion in a bone marrow metastatic myeloma model. Clin Exp Metastasis. 1999; 17(7):623–629. [PubMed: 10845562]

4. Kim MS, Day CJ, Selinger CI, Magno CL, Stephens SR, Morrison NA. MCP-1-induced human osteoclast-like cells are tartrate-resistant acid phosphatase, NFATc1, and calcitonin receptor-positive but require receptor activator of NFkappaB ligand for bone resorption. The Journal of biological chemistry. 2006; 281(2):1274–1285. [PubMed: 16280328]

5. Giuliani N, Rizzoli V. Myeloma cells and bone marrow osteoblast interactions: role in the development of osteolytic lesions in multiple myeloma. Leukemia & lymphoma. 2007; 48(12): 2323–2329. [PubMed: 18067006]

6. Hiruma Y, Honjo T, Jelinek D, Windle JJ, Shin J, Roodman GD, et al. Increased signaling through p62 in the marrow microenvironment increases myeloma cell growth and osteoclast formation. Blood. 2009; 113(20):4894–4902. [PubMed: 19282458]

7. Teramachi J, Windle JJ, Roodman D, Kurihara N. The ZZ Domain of Sequestosome-1/p62 Plays An Important Role In Stromal Cell Support of Myeloma Cell Growth and Osteoclast Formation. ASH Annual Meeting Abstracts. 2010; 116(21):128.

8. Yang, P.; Teramachi, J.; Feng, R.; Wang, L.; Beumer, JH.; Eiseman, JL., et al. A Novel Chemical Inhibitor Targeting Sequestosme-1/p62 Suppresses Multiple Myeloma Cell Growth and Osteoclast Formation. Poster presentation at the 2014 AAPS Annual Meeting and Exposition; November, 2014; San Diego, CA Poster T3045. 2014.

9. Teramachi J, Myint KZY, Feng R, Xie X, Windle JJ, Roodman D, et al. Blocking the ZZ Domain of Sequestosome 1/p62 Suppress the Enhancement of Myeloma Cell Growth and Osteoclast Formation by Marrow Stromal Cells. ASH Annual Meeting Abstracts. 2011; 118(21):888.

10. Kurihara N, Chenu C, Miller M, Civin C, Roodman GD. Identification of committed mononuclear precursors for osteoclast-like cells formed in long term human marrow cultures. Endocrinology. 1990; 126(5):2733–2741. [PubMed: 2184023]

11. Kurihara N, Civin C, Roodman GD. Osteotropic factor responsiveness of highly purified populations of early and late precursors for human multinucleated cells expressing the osteoclast phenotype. Journal of bone and mineral research : the official journal of the American Society for Bone and Mineral Research. 1991; 6(3):257–261.

12. D'Souza S, del Prete D, Jin S, Sun Q, Huston AJ, Kostov FE, et al. Gfi1 expressed in bone marrow stromal cells is a novel osteoblast suppressor in patients with multiple myeloma bone disease. Blood. 2011; 118(26):6871–6880. [PubMed: 22042697]

13. Cumova J, Kovarova L, Potacova A, Buresova I, Kryukov F, Penka M, et al. Optimization of immunomagnetic selection of myeloma cells from bone marrow using magnetic activated cell sorting. International journal of hematology. 2010; 92(2):314–319. [PubMed: 20694533]

14. Cackowski FC, Anderson JL, Patrene KD, Choksi RJ, Shapiro SD, Windle JJ, et al. Osteoclasts are important for bone angiogenesis. Blood. 2010; 115(1):140–149. [PubMed: 19887675]

15. D'Argenio, D.; Schumitzky, A.; Wang, X. ADAPT 5 User's Guide: Pharmacokinetic/ Pharmacodynamic Systems Analysis Software. Los Angeles, CA: Biomedical Simulations Resource; 2014.

16. Kurihara N, Hiruma Y, Yamana K, Michou L, Rousseau C, Morissette J, et al. Contributions of the measles virus nucleocapsid gene and the SQSTM1/p62(P392L) mutation to Paget's disease. Cell metabolism. 2011; 13(1):23–34. [PubMed: 21195346]

17. National Research Council (U.S.). Committee for the Update of the Guide for the Care and Use of Laboratory Animals. Institute for Laboratory Animal Research (U.S.). National Academies Press (U.S.). Washington D.C.: National Academies Press; 2011. Guide for the care and use of laboratory animals. Available from: http://www.ncbi.nlm.nih.gov/books/NBK54050 ebrary http://site.ebrary.com/id/10443276 National Academies Press http://www.nap.edu/catalog.php?record_id=12910 National Academies Press http://www.nap.edu/catalog.php?record_id=12910 - tochttp://www.ncbi.nlm.nih.gov/bookshelf/br.fcgi?book=nap12910http://grants.nih.gov/grants/olaw/Guide-for-the-Care-and-use-of-laboratory-animals.pdf.

18. Mohammad KS, Javelaud D, Fournier PG, Niewolna M, McKenna CR, Peng XH, et al. TGF-beta-RI kinase inhibitor SD-208 reduces the development and progression of melanoma bone metastases. Cancer research. 2011; 71(1):175–184. [PubMed: 21084275]

19. Mitsiades CS, Mitsiades NS, Munshi NC, Richardson PG, Anderson KC. The role of the bone microenvironment in the pathophysiology and therapeutic management of multiple myeloma:

interplay of growth factors, their receptors and stromal interactions. Eur J Cancer. 2006; 42(11): 1564–1573. [PubMed: 16765041]

20. Ye H, Arron JR, Lamothe B, Cirilli M, Kobayashi T, Shevde NK, et al. Distinct molecular mechanism for initiating TRAF6 signalling. Nature. 2002; 418(6896):443–447. [PubMed: 12140561]
21. Sanz L, Sanchez P, Lallena MJ, Diaz-Meco MT, Moscat J. The interaction of p62 with RIP links the atypical PKCs to NF-kappaB activation. Embo J. 1999; 18(11):3044–3053. [PubMed: 10356400]
22. Ducy P, Zhang R, Geoffroy V, Ridall AL, Karsenty G. Osf2/Cbfa1: a transcriptional activator of osteoblast differentiation. Cell. 1997; 89(5):747–754. [PubMed: 9182762]
23. Xu G, Liu K, Anderson J, Patrene K, Lentzsch S, Roodman GD, et al. Expression of XBP1s in bone marrow stromal cells is critical for myeloma cell growth and osteoclast formation. Blood. 2012; 119(18):4205–4214. [PubMed: 22427205]
24. Tai YT, Podar K, Mitsiades N, Lin B, Mitsiades C, Gupta D, et al. CD40 induces human multiple myeloma cell migration via phosphatidylinositol 3-kinase/AKT/NF-kappa B signaling. Blood. 2003; 101(7):2762–2769. [PubMed: 12433678]
25. Hideshima T, Chauhan D, Schlossman R, Richardson P, Anderson KC. The role of tumor necrosis factor alpha in the pathophysiology of human multiple myeloma: therapeutic applications. Oncogene. 2001; 20(33):4519–4527. [PubMed: 11494147]
26. Puls A, Schmidt S, Grawe F, Stabel S. Interaction of protein kinase C zeta with ZIP, a novel protein kinase C-binding protein. Proceedings of the National Academy of Sciences of the United States of America. 1997; 94(12):6191–6196. [PubMed: 9177193]
27. Xie X-Q, Yang P, Teramachi J, Feng R, Myint K-Z, Beumer JH, et al. A novel chemical inhibitor targeting Sequestosome-1/p62 suppresses multiple myeloma cell growth and osteoclast formation. Nature Chemical Biology. Submitted 2014.
28. Gilbert L, He X, Farmer P, Boden S, Kozlowski M, Rubin J, et al. Inhibition of osteoblast differentiation by tumor necrosis factor-alpha. Endocrinology. 2000; 141(11):3956–3964. [PubMed: 11089525]
29. Duran A, Serrano M, Leitges M, Flores JM, Picard S, Brown JP, et al. The atypical PKC-interacting protein p62 is an important mediator of RANK-activated osteoclastogenesis. Dev Cell. 2004; 6(2):303–309. [PubMed: 14960283]
30. Jin Z, Li Y, Pitti R, Lawrence D, Pham VC, Lill JR, et al. Cullin3-based polyubiquitination and p62-dependent aggregation of caspase-8 mediate extrinsic apoptosis signaling. Cell. 2009; 137(4): 721–735. [PubMed: 19427028]
31. Rodriguez A, Duran A, Selloum M, Champy MF, Diez-Guerra FJ, Flores JM, et al. Mature-onset obesity and insulin resistance in mice deficient in the signaling adapter p62. Cell metabolism. 2006; 3(3):211–222. [PubMed: 16517408]
32. Painuly U, Kumar S. Efficacy of bortezomib as first-line treatment for patients with multiple myeloma. Clinical Medicine Insights Oncology. 2013; 7:53–73. [PubMed: 23492937]
33. Kapoor P, Ramakrishnan V, Rajkumar SV. Bortezomib combination therapy in multiple myeloma. Seminars in hematology. 2012; 49(3):228–242. [PubMed: 22726546]

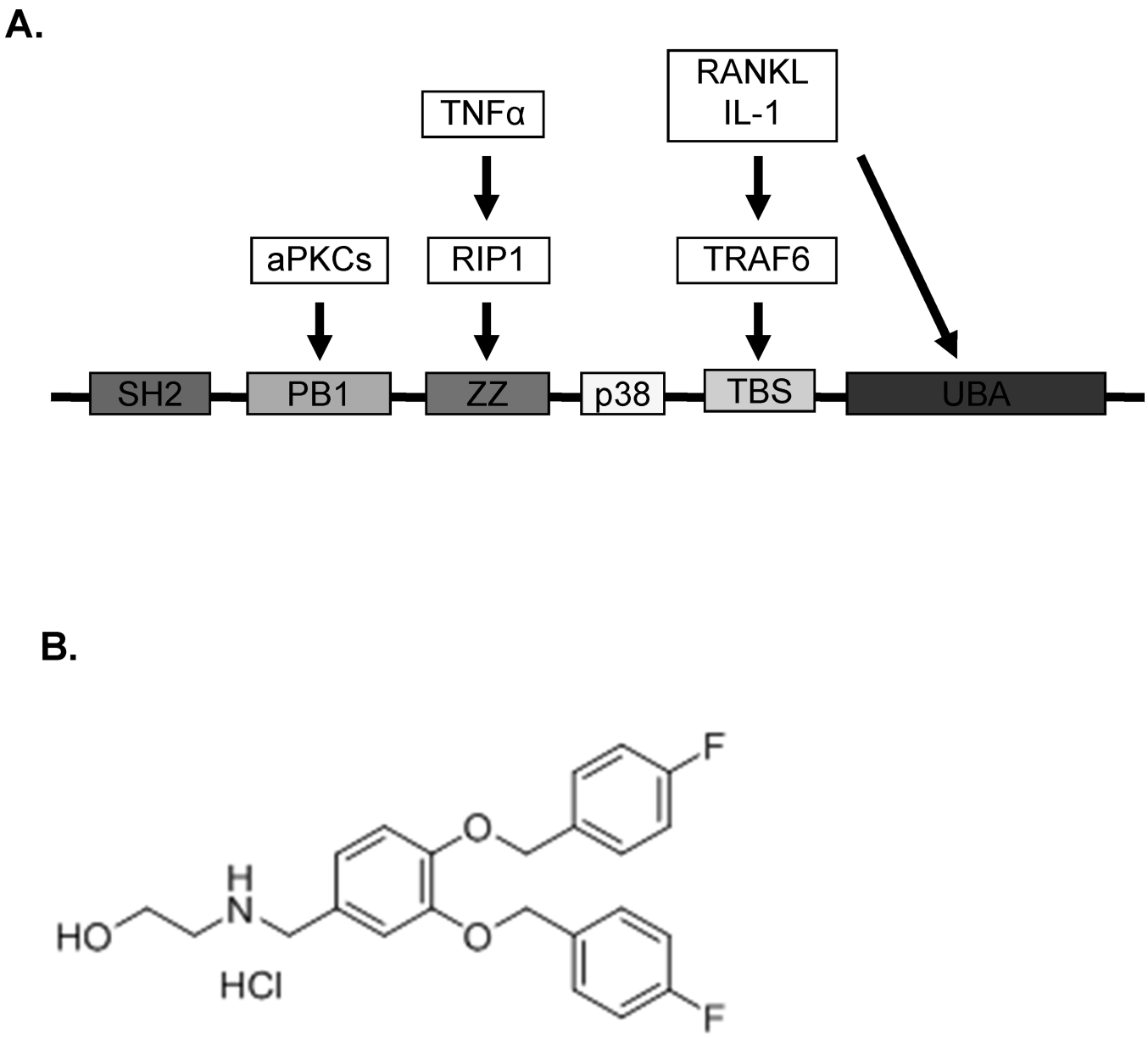

Figure 1.

A Binding domains of p62. Sequestosome 1 (p62) is an adapter protein without intrinsic enzymatic activity that serves as a platform for the formation of many of the signaling complexes that result in NFκB and p38 MAPK activation in the marrow microenvironment of MM patients. The ZZ domain of p62 is required for BMSC support of MM cell growth and acts as a signaling hub for the formation of BMSC signaling complexes activated by MM cells and TNFα. SH2 = Src homology 2, aPKCs = atypical protein kinase C, PB1 = Phox and Bem1p, RIP1 = receptor-interacting protein-1, TRAF6 = TNF receptor-associated factor 6, TBS = TRAF6 binding site, UBA = ubiquitin-associated domain. **1B: Structure of XRK3F2**.

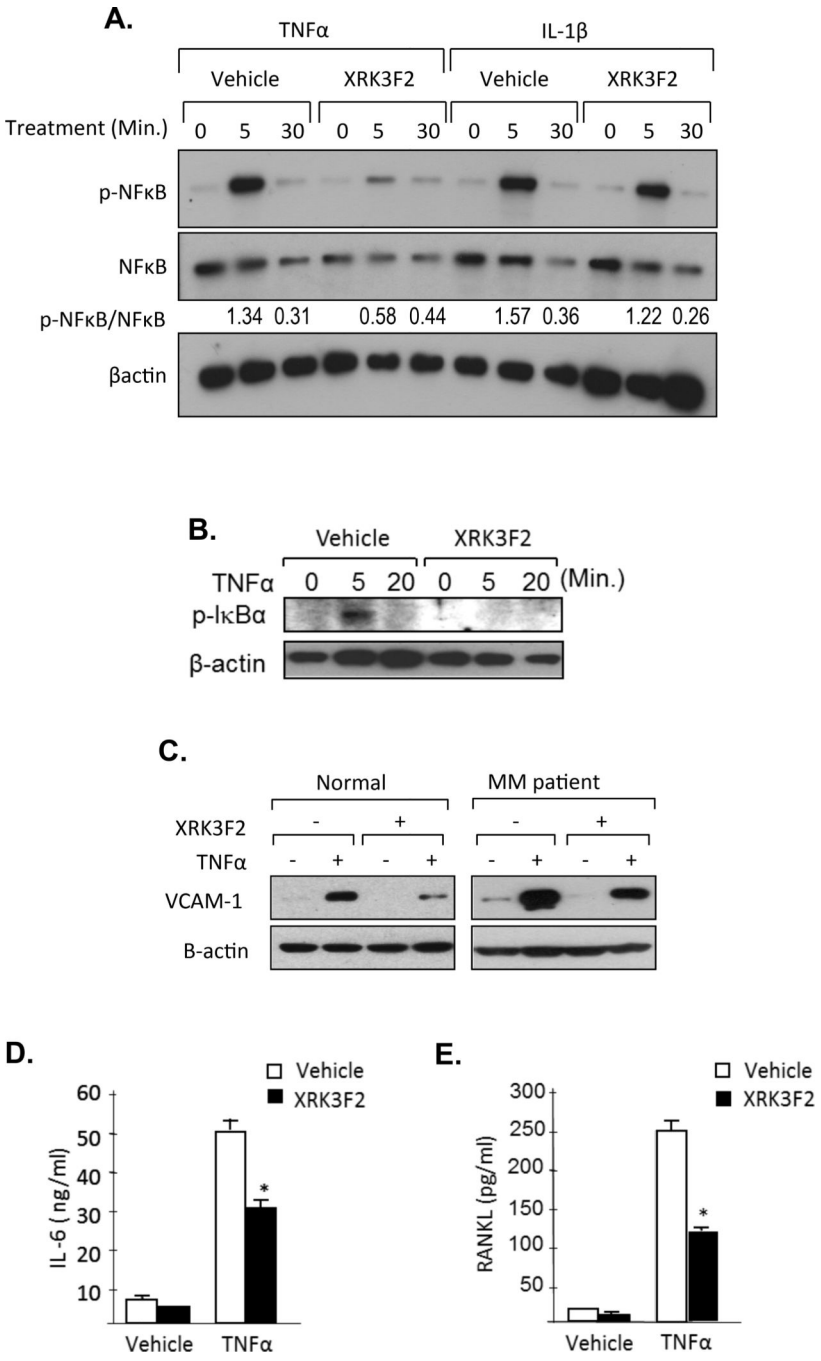

Figure 2. XRK3F2 blocks TNFα-induced signaling processes in MM patient BMSC and MM cells

A. XRK3F2 blocks TNFα but not IL-1β stimulated NFkB phosphorylation on MM patient BMSC. MM patient BMSC were pre-treated with 10mg/ml of XRK3F2 or vehicle (0.1% DMSO) for 3 hours. Cells were then stimulated with 10ng/ml of TNFα or IL-1β for the indicated times. Phospho-NFκB (p-NFκB) and NFκB were assayed by Western blot using anti-phospho-NFκB and anti-NFκB antibodies. The ratio of p-NFκB to total NFκB at the 5 and 30-minute time points for each treatment condition is shown. **B. XRK3F2**

inhibited p-IκBα activation by TNFα in MM patient BMSCs. BMSCs were pre-treated with XRK3F2. For assay of degradation of IκBα, cells were stimulated with 10ng/ml of TNFα for the indicated times and the cell lysates were collected. Total IκBα were assayed by Western blot using an IκBα antibody. **C. VCAM-1 expression on representative normal and MM patient BMSCs.** VCAM-1 expression was assayed by Western blotting. BMSCs were cultured with and without TNFα and XRK3F2 for 48 hours. Cell lysates were then collected and VCAM-1 expression measured using an anti-VCAM-1 antibody. **D. IL-6 production by MM patient BMSCs.** BMSCs were cultured with and without TNFα and XRK3F2 for 48 hours. Cell culture media were collected and IL-6 production measured using an IL-6 ELISA kit. Data are shown as the mean ± SD (n=3). *$p<0.01$ compared to non-treatment control culture. **E. RANKL production by MM patient BMSCs.** BMSCs were cultured with and without TNFα and XRK3F2 for 48 hours. Cell culture media were collected and RANKL production measured using a RANKL ELISA kit. Data are shown as the mean ± SD (n=3). * $p<0.01$ compared to vehicle treatment control culture.

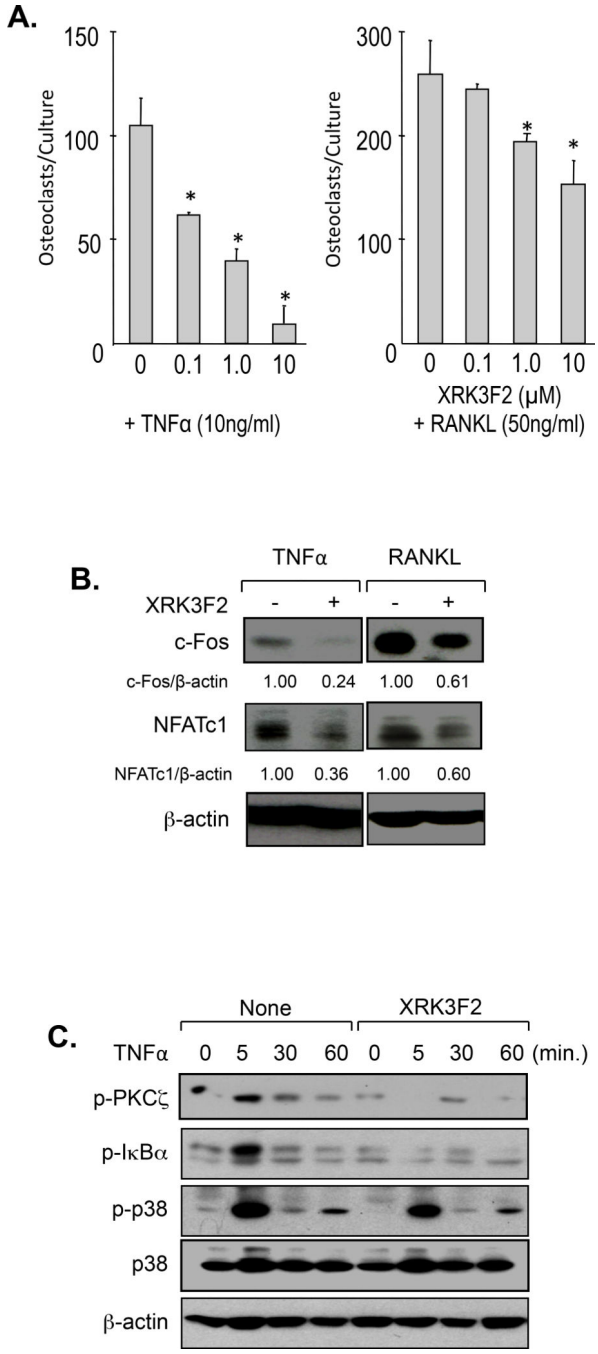

Figure 3. Effects of XRK3F2 on human OCL formation

A. XRK3F2 in combination with TNFα or RANKL significantly reduced human OCL formation. Human CD11b$^+$ mononuclear cells (OCL precursors) derived from human bone marrow samples were cultured in α-MEM containing 20% horse serum with TNFα or RANKL and various doses of XRK3F2. Multi-nucleated osteoclasts were stained for 23C6, which recognizes CD51/61. Data are shown as mean ± SD (n=5). ** $p<0.01$* compared to non-treatment cultures. **B. XRK3F2 blocked c-Fos and NFATc1 activation.** CD11b$^+$ cells were pre-treated with XRK3F2 and OCL precursors were stimulated with TNFα or RANKL

in the absence or presence XRK3F2 for 48 hours. The cell lysates were collected and assayed for expression of c-Fos and NFATc1 using anti-c-Fos and anti-NFATc1 antibodies.

C. XRK3F2 inhibited p-PKCζ and p-IκBα activation in OCL precursors. $CD11b^{+}$ cells were pre-treated with XRK3F2 and stimulated with 10ng/ml of TNFα for the times indicated. Phospho-PKCς, IκBα and p38 MAPK were assayed using anti-phospho PKCς, anti-phospho IκBα and anti-phospho p38 MAPK antibodies.

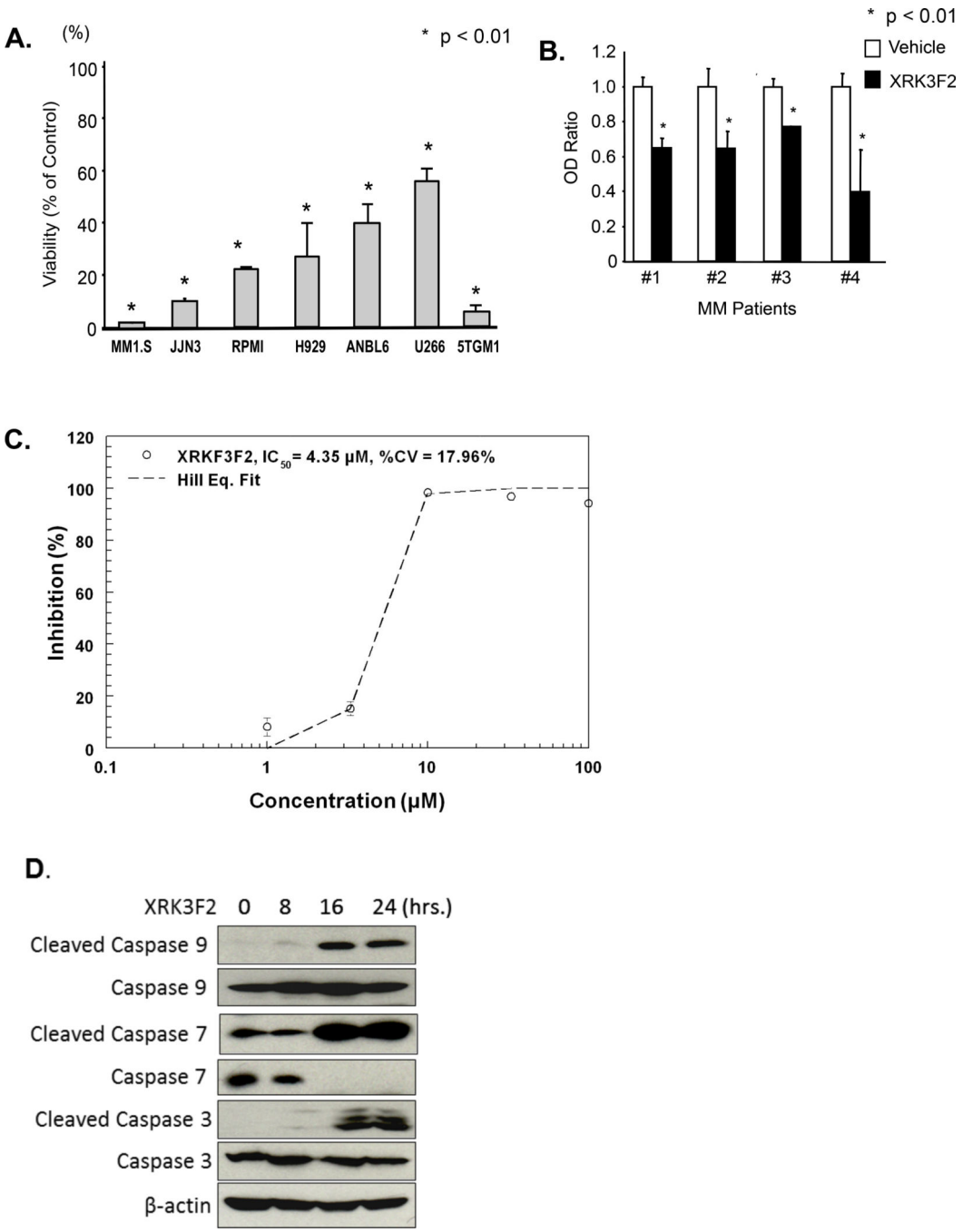

Figure 4. XRK3F2 blocks MM cell growth

A. Effect of XRK3F2 on human MM cell lines and the murine 5TGM1 cell line. Each cell line was treated with 10µM XRK3F2 and analyzed by MTT assay. Data are shown as the mean ± SD (n=5). **p<0.01* compared to cell cultures treated with vehicle. **B. XRK3F2 blocks primary MM cell growth**. $CD138^+$ cells from MM patients were treated with 10µM of XRK3F2 for 48 hours and analyzed for cell viability by MTT assay. Data are shown as the mean ± SD (n=5). **p<0.01* compared to vehicle treated cultures. **C. The IC_{50} for PY1-32 against 5TGM1-gfp murine multiple myeloma cells in a 72 hour MTT assay**

was 4.35 μM. D. XRK3F2 induced cleavage of caspase 9, 7 and 3 in MM1.S cells. MM1.S cells were cultured with 10μM XRK3F2 for the indicated time and cell lysates were collected. Cleaved and uncleaved caspases 9, 7 and 3 were detected by Western blotting using anti-cleaved and uncleaved caspase 9, 7 and 3 specific antibodies.

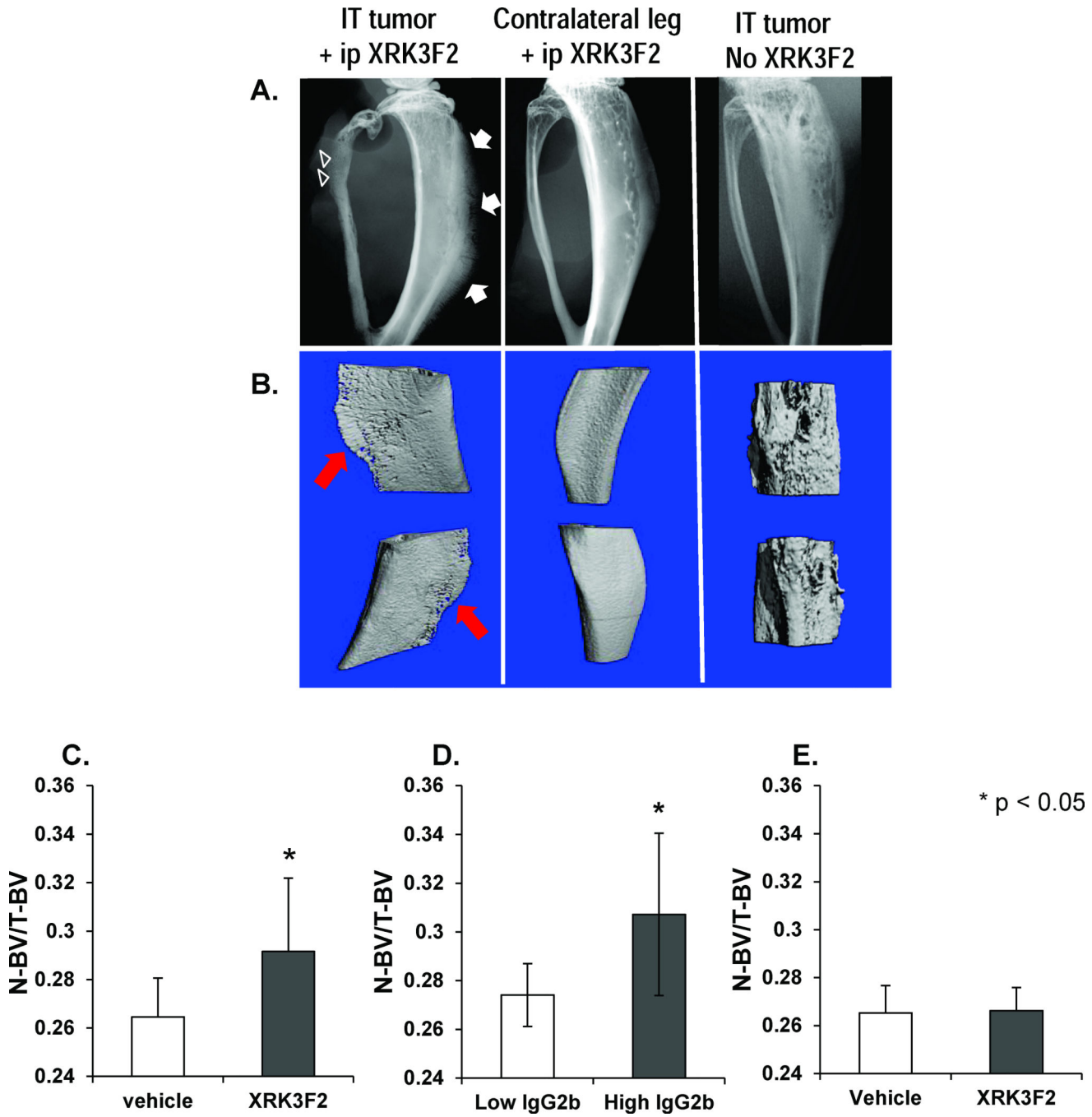

Figure 5. XRK3F2 treatment results in new bone formation in an *in vivo* model of MM bone disease

A. Representative radiographic images of fixed tibiae from animals inoculated with 5TGM1 MM cells (left, center) and XRK3F2, and animals that received IT 5TGM1 injections in the absence of XRK3F2. The tibia shown with 5TGM1 inoculation and XRK3F2 exposure (left) has an aggressive periosteal reaction in the form of delicate rays of periosteal bone that extend away from the bone perpendicularly – creating a “hair on end” appearance (arrow). In addition, a permeative pattern of bone destruction is noted in the

fibula (arrowheads). This pattern of bone destruction is associated with rapid growth of the inciting agent, such as in cases of bone metastases and myeloma. In contrast, the center x-ray image (tibia from the contralateral (non-5TGM1 injected) leg of an animal with MM and treated with XRK3F2 has no evidence of a periosteal reaction, though osteopenia is evident. Finally, no periosteal reaction is seen on x-ray of a tibia treated with IT 5TGM1 cells but no XRK3F2. Lytic lesions are visible. **B. μCT images of new bone formation.** Fixed tibiae were scanned using a microCT system (vivaCT 40, Scanco Medical). Composite μCT images of the volume of interest for each tibia are shown, and correlate with the bones whose x-ray images are above. New bone formation can clearly be seen along the tibial diaphysis of the tibia that had direct MM cell inoculation and XRK3F2 exposure. No new bone formation is seen in either the contralateral leg of an animal that did have XRK3F2 exposure (center) or the MM-injected control that did not have XRK3F2 exposure. **C. New bone volume is increased in all XRK3F2 treated mice.** To compare new bone formation between vehicle and XRK3F2 treated animals, a global threshold was applied to delineate newly formed bone (330) from total bone (180) from surrounding soft tissue and water. The ratio of new (N) bone volume (BV) as compared to total BV was increased in all XRK3F2-F_2 treated mice regardless of IgG_{2b} level ($p=0.015$). *$p < 0.05$ compared to vehicle treated animals. **D. XRK3F2 treated mice with high tumor burden had more new bone formation.** XRK3F2 treated mice with high monoclonal IgG_{2b} levels (a marker of tumor burden) had significantly more new bone formation than animals with low IgG_{2b} levels ($p=0.018$). *$p < 0.05$ compared to low IgG_{2b} animals. **E: Effects of XRK3F2 on uninvolved bone.** To evaluate if the effect of XRK3F2 on new bone formation is systemic or occurs only in the presence of tumor, we compared N-BV/T-BV in the non-tumor bearing (left) tibiae of animals treated with vehicle or XRK3F2. New bone volume did not differ significantly between the groups. Data are shown as mean ± SD.

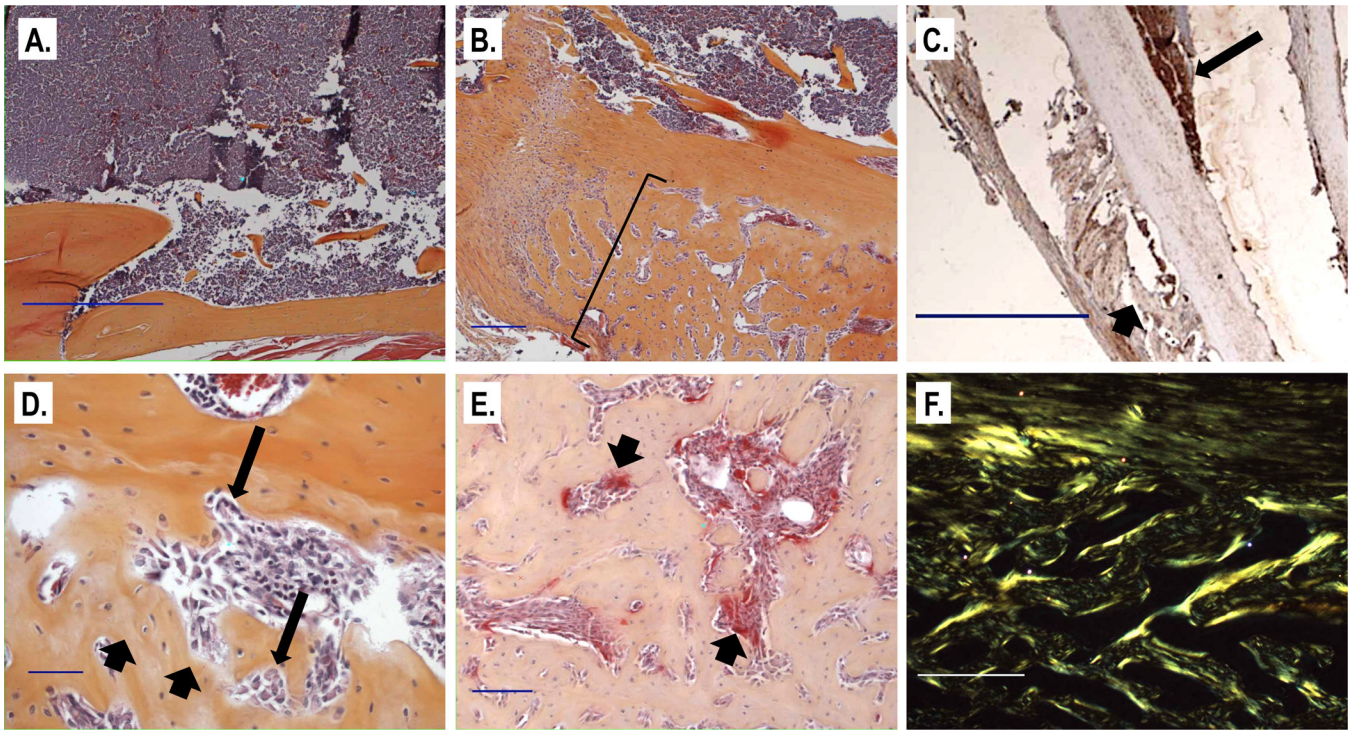

Figure 6. Representative histologic sections from XRK3F2 treated animals with new bone formation (B-F) and a vehicle treated animal without new bone formation (A)

All sections shown are from animals that received MM cell inoculation. **A.** Sections from 5TGM1-inoculated mice that did not receive XRK3F2 demonstrate a significant plasma cell infiltrate in the marrow space, as expected, and normal cortical morphology with no evidence of new bone formation (x50, scale bar = 500μ). **B.** Sections from mice treated with XRK3F2 stained with H&E show abundant new bone formation along the periosteal surface of the tibia (bracket) inoculated with 5TGM1 cells (×50, scale bar = 100μ). **C.** anti-GFP immunohistochemistry confirmed that plasma cell (5TGM1-tk-gfp) infiltration (long arrow) in the marrow space was in close proximity to areas of new bone formation (short arrow) (×16, scale bar indicates 500μ). **D.** Higher magnification demonstrates new bone (short arrows) and active osteoblasts (long arrows) (×200, scale bar = 100μ). **E.** TRAP stained section from a representative section with new bone formation shows the presence of red-staining osteoclasts (arrows) along the new bone surface (×100, scale bar = 100μ). **F.** Polarizing microscopy demonstrates a disorganized (woven) arrangement of the newly laid bone, indicating that this bone was laid rapidly. (×100, scale bar = 100 microns. Collagen fibrils are green.)

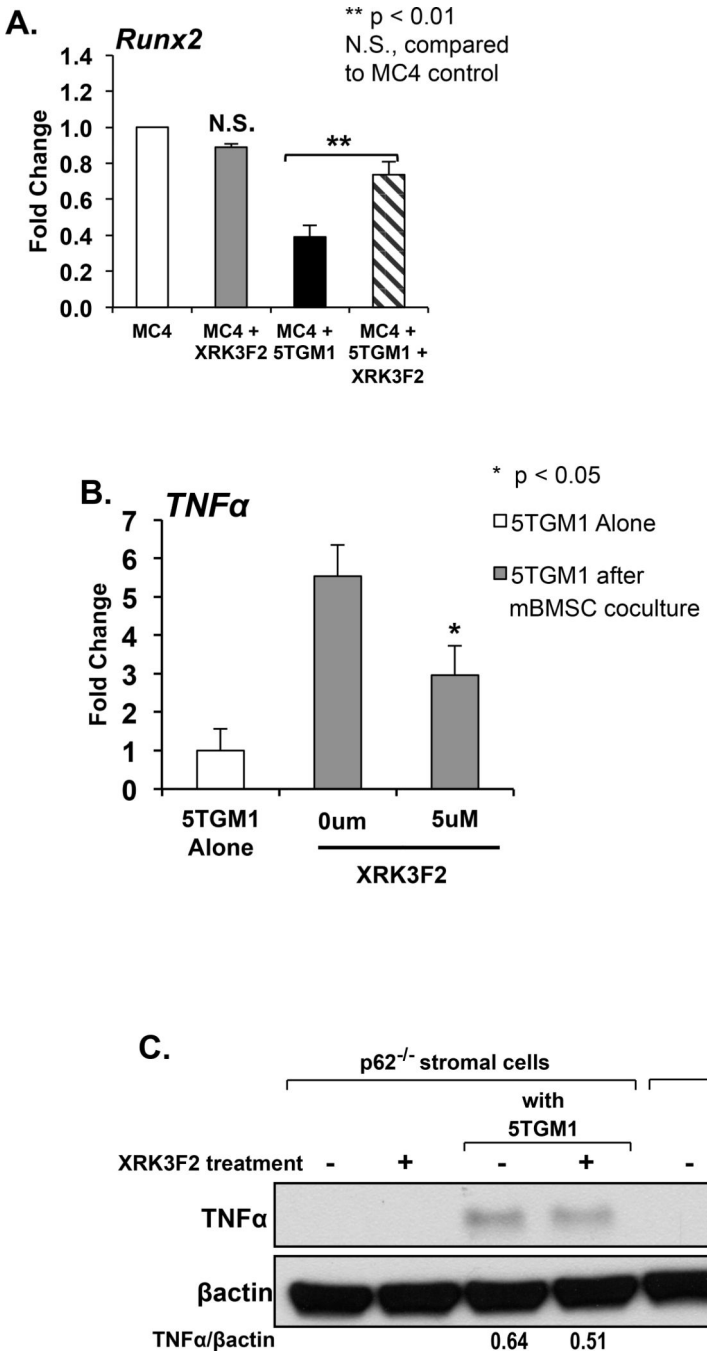

Figure 7. XRK3F2 blocks Runx2 downregulation and TNFα induction in cocultures of MM cells and BMSC expressing p62

A. XRK3F2 blocks suppression of OB differentiation in MM cell – stromal cell coculture. MC4 (pre-osteoblast) cells were directly cocultured with 5TGM1 cells under osteogenic conditions in the presence and absence of XRK3F2 for 72 hours. 5TGM1 cells were then removed by washing and MC4 cell lysates prepared. MC4 Runx2 mRNA production was analyzed by qPCR using the comparative $2^{-\Delta\Delta Ct}$ method. Data is normalized to GAPDH and presented as mean ± SD for a typical experiment. Runx2 expression was not

suppressed in XRK3F2 treated MC4 cells cocultured with 5TGM1 cells. **p<0.01, N.S. no significant difference compared to MC4 control. **B. XRK3F2 reduces upregulation of TNFα in MM cells cocultured with BMSC.** 5TGM1 cells were cultured alone or in the presence of primary mBMSC cells and XRK3F2 for 48hours. At the end of the culture period, 5TGM1 cells were washed from the mBMSC and 5TGM1 cell lysates prepared. TNFα production was analyzed by qPCR and normalized to 18S. XRK3F2 significantly decreased mBMSC-induced upregulation of TNFα in 5TGM1 cells. **C. XRK3F2 reduced the increase in stromal cell expression of TNFα induced by coculture with MM cells.** We used BMSC from p62KO ($p62^{-/-}$) and p62 heterozygote ($p62^{+/-}$) littermates to evaluate if XRK3F2 alters the increased stromal cell production of TNFα following coculture with MM cells, and if the effect of XRK3F2 is mediated by p62. $p62^{+/-}$ and $p62^{-/-}$ BMSC were incubated with and without 5TGM1 cells in the presence and absence of XRK3F2 for 12 hours. Following coculture, 5TGM1 cells were washed from the BMSC, and TNFα expression was assessed by Western blot. TNFα was undetectable in BMSC cultured alone, and upregulated to a greater extent in $p62^{+/-}$ than $p62^{-/-}$ BMSC following coculture with 5TGM1 MM cells. TNFα expression was also undetectable in XRK3F2 treated BMSC cultured in the absence of MM cells. Coculture of $p62^{+/-}$ BMSCs in the presence of XRK3F2 reduced the increase in TNFα expression in BMSC while XRK3F2 did not greatly alter the upregulation of TNFα in $p62^{-/-}$ BMSC cocultured with MM cells.

Table

Patient Characteristics

ID	Age	Gender	Stage	
1	76	Female	IIA	Relapsed Disease
2	77	Female	III	Relapsed Disease
3	65	Male	III	Relapsed Disease
4	69	Male	IIIA	Relapsed Disease